Magnon-Driven Domain-Wall Motion with the Dzyaloshinskii-Moriya Interaction

Weiwei Wang,[1] Maximilian Albert,[1] Marijan Beg,[1] Marc-Antonio Bisotti,[1] Dmitri Chernyshenko,[1] David Cortés-Ortuño,[1] Ian Hawke,[2] and Hans Fangohr[1,*]

[1]*Engineering and the Environment, University of Southampton, SO17 1BJ Southampton, United Kingdom*

[2]*Mathematical Sciences, University of Southampton, SO17 1BJ Southampton, United Kingdom*

(Received 27 June 2014; published 26 February 2015)

We study domain-wall (DW) motion induced by spin waves (magnons) in the presence of the Dzyaloshinskii-Moriya interaction (DMI). The DMI exerts a torque on the DW when spin waves pass through the DW, and this torque represents a linear momentum exchange between the spin wave and the DW. Unlike angular momentum exchange between the DW and spin waves, linear momentum exchange leads to a rotation of the DW plane rather than a linear motion. In the presence of an effective easy plane anisotropy, this DMI induced linear momentum transfer mechanism is significantly more efficient than angular momentum transfer in moving the DW.

DOI: 10.1103/PhysRevLett.114.087203 PACS numbers: 75.30.Ds, 75.60.Ch, 75.78.Cd, 85.75.-d

The manipulation of domain-wall (DW) motion has been extensively studied in the past few years due to potential applications in logic devices and data storage technology [1–5]. A DW can be driven by an applied field [6], microwaves [7], spin transfer torque [8], and spin waves (magnons) [9–11]. Spin waves can drive the DW effectively since they carry magnonic spin current. In general, when the spin waves travel through the DW, the DW acquires a negative velocity—relative to the propagation direction of the spin waves—due to conservation of angular momentum [11], although positive velocities have been observed in micromagnetic simulations at special frequencies [10,12–14].

Angular momentum conservation plays a crucial role in spin wave induced DW motion: when the spin wave passes through the DW, the magnonic spin current changes its sign, which generates a torque and the DW moves in order to absorb this torque. Magnons can be considered as particles with angular momentum $\pm\hbar$ and linear momentum $\hbar k$ [11]. When the spin wave is reflected, linear momentum is transferred to the DW which results in DW motion [12,15]. The difference between these two mechanisms is that the DW moves in opposite directions [15,16]. In this Letter we demonstrate, by using micromagnetic simulations and a one-dimensional (1D) analytical DW model, that spin waves passing through a domain wall in the presence of a Dzyaloshinskii-Moriya interaction (DMI) and an easy-plane anisotropy drive the domain wall very effectively. We attribute this to linear momentum transfer and show that this effect can be more efficient than the better known angular momentum transfer by an order of magnitude.

The DMI is an antisymmetric interaction induced by spin-orbit coupling due to broken inversion symmetry in lattices or at the interface of magnetic films [17]. The DMI can lead to chiral magnetic orders such as Skyrmions and spin spirals [17–20]. In addition, the DMI has brought new phenomena for DW dynamics driven by fields [21] or charge currents [22]. The DMI has been found both for magnetic interfaces [20] and bulk materials such as MnSi [23] and FeGe [24]. In this work we focus on bulk DMI with micromagnetic energy density $\varepsilon_{\mathrm{DMI}} = D\mathbf{m}\cdot(\nabla\times\mathbf{m})$ where D is the DMI constant and $\mathbf{m}$ is the normalized magnetization.

We consider a quasi-1D nanowire with the exchange interaction, DMI, and two effective anisotropies. One anisotropy K is the uniaxial anisotropy along the x axis, and the other effective $K_\perp$ is an easy xy-plane anisotropy. The combined anisotropies can be considered as a model of overall effect including the demagnetization field, surface, or magnetoelastic anisotropy [24,25]. The total free energy for the wire along the x axis is

$$E = S\int [A(\nabla\mathbf{m})^2 - Km_x^2 + K_\perp m_z^2 + \varepsilon_{\mathrm{DMI}}]dx, \qquad (1)$$

where S is the cross-sectional area of the wire and A is the exchange constant.

The dynamics of the magnetization $\mathbf{m}$ is governed by the Landau-Lifshitz-Gilbert (LLG) equation

$$\frac{\partial\mathbf{m}}{\partial t} = -\gamma\mathbf{m}\times\mathbf{H}_{\mathrm{eff}} + \alpha\mathbf{m}\times\frac{\partial\mathbf{m}}{\partial t}, \qquad (2)$$

where $\gamma(>0)$ is the gyromagnetic ratio and α is the Gilbert damping. The effective field $\mathbf{H}_{\mathrm{eff}}$ is calculated as the functional derivative $\mathbf{H}_{\mathrm{eff}} = -1/(\mu_0 M_s)\delta E/\delta\mathbf{m} = 2/(\mu_0 M_s)[A\nabla^2\mathbf{m} - D\nabla\times\mathbf{m} + Km_x\mathbf{e}_x - K_\perp m_z\mathbf{e}_z]$ with M_s the saturation magnetization and μ_0 the vacuum permeability.

The typical DW structures described by the energy [Eq. (1)] for the case $D = 0$ are head-to-head and tail-to-tail DWs, and the former is shown in Fig. 1(a). By using spherical coordinates $\theta = \theta(x)$ and $\phi = \phi(x)$, the magnetization unit vector $\mathbf{m}$ is expressed as

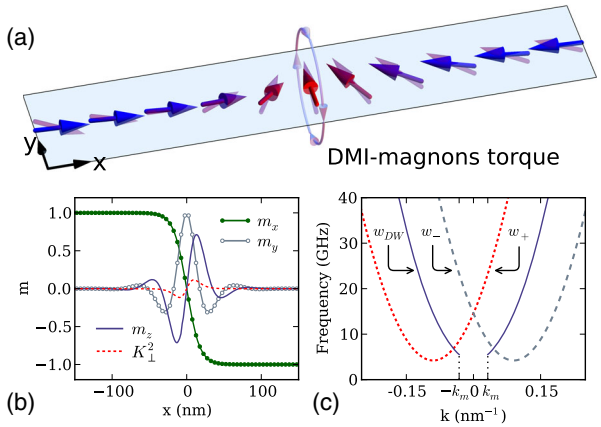

FIG. 1 (color online). (a) Illustration of the head-to-head DW in the nanowire using red-blue opaque arrows. The translucent purple arrows represent a spin wave excitation. The DMI exerts a torque to change the DW tilt angle when spin waves pass through the DW. (b) DW profile using Eq. (5) with parameters $A = 8.78 \times 10^{-12}$ J/m, $K = 1 \times 10^5$ J/m^3, $D = 1.58 \times 10^{-3}$ J/m^2, $K_\perp = 0$ and $\Phi = 0$. The red dashed line shows the simulation data for m_z with $K_\perp^2 = 6 \times 10^5$ J/m^3: the easy-plane anisotropy favors a reduced m_z. (c) The dispersion relations inside and outside the DW.

$\mathbf{m} = (\cos\theta, \sin\theta\cos\phi, \sin\theta\sin\phi)$, and the total micromagnetic energy [Eq. (1)] reads

$$E = S\int [A(\theta'^2 + \sin^2\theta\phi'^2) - D\phi'\sin^2\theta + K\sin^2\theta(1 + \kappa\sin^2\phi)]dx, \quad (3)$$

where $\kappa = K_\perp/K$ and $'$ represents the derivative with respect to x. In the equilibrium state, the energy [Eq. (3)] must be minimal, and thus we arrive at two coupled differential equations for θ and ϕ by using standard variational calculus,

$$2A\theta'' = \sin 2\theta(A\phi'^2 + K(1 + \kappa\sin^2\phi) - D\phi'),$$
$$\sin\theta(2A\phi'' - K_\perp \sin 2\phi) = 2\cos\theta(D - 2A\phi')\theta'. \quad (4)$$

The corresponding boundary conditions are $\theta' = 0$ and $(\phi' - 1/\xi)\sin^2\theta = 0$ for $x = \pm\infty$ (see Supplemental Material [26]) where $\xi = 2A/D$ is the characteristic length [20]. We are searching for the head-to-head DW solution; therefore, the ansatz $\cos\theta = -\tanh[(x - x_0)/\Delta]$ is used, where Δ is the DW width and x_0 is the DW center. Initially, we consider the case of $\kappa = 0$ (i.e., $K_\perp = 0$) which preserves the rotational symmetry. We assume that ϕ is a linear function of space x, i.e., $\phi(x) = (x - x_0)/\xi + \Phi$ where Φ is the DW tilt angle. Inserting back into Eq. (4) we obtain $\Delta = \sqrt{A/(K - A/\xi^2)}$. In the absence of the DMI, the DW width reduces to $\Delta_0 = \sqrt{A/K}$ which is the well-known Bloch wall width. Therefore, the static one-dimensional head-to-head DW profile can be expressed as [22]

$$m_x = -\tanh(x/\Delta),$$
$$m_y = \mathrm{sech}(x/\Delta)\cos(x/\xi + \Phi),$$
$$m_z = \mathrm{sech}(x/\Delta)\sin(x/\xi + \Phi), \quad (5)$$

where we have chosen $x_0 = 0$. Figure 1(b) shows the DW profile using Eq. (5) for $K_\perp = 0$ with lines, and the red dashed line depicts the micromagnetic simulation result of m_z for $K_\perp^2 = 6 \times 10^5$ J/m^3. The rotational symmetry breaks for $K_\perp > 0$ and the z component of the magnetization m_z is suppressed by the easy plane anisotropy. The DW configuration [Eq. (5)] is not stable if the DMI constant is larger than the critical value $D_c = 2\sqrt{AK}$ [22], and the presence of $K_\perp > 0$ increases this threshold.

We assume that the spin wave can be described by a small fluctuation $u = u(x)$ and $v = v(x)$ around $\mathbf{m}_0$, where $\mathbf{m}_0 = (\cos\theta_0, \sin\theta_0\cos\phi_0, \sin\theta_0\sin\phi_0)$ is the static domain-wall profile Eq. (5),

$$\mathbf{m} = \mathbf{m}_0 + [u(x)\mathbf{e}_\theta + v(x)\mathbf{e}_\phi]e^{-iwt}, \quad (6)$$

where $\sqrt{u^2 + v^2} \ll 1$, $\mathbf{e}_\phi = (0, -\sin\phi_0, \cos\phi_0)$, $\mathbf{e}_\theta = (-\sin\theta_0, \cos\theta_0\cos\phi_0, \cos\theta_0\sin\phi_0)$, and ω is the spin wave frequency. By following the treatment in Ref. [11], we obtain for the $K_\perp = 0$ case,

$$Av'' - \tilde{K}v\cos(2\theta_0) = -iu\omega/\gamma_0,$$
$$Au'' - \tilde{K}u\cos(2\theta_0) = iv\omega/\gamma_0, \quad (7)$$

where we define $\tilde{K} = K - D^2/(4A)$ and $\gamma_0 = 2\gamma/(\mu_0 M_s)$. By introducing the complex variable $\psi = u - iv$, Eq. (7) can be written as a time-independent Schrödinger-type equation with reflectionless potential [27,28],

$$\hat{H}\psi(\zeta) = (1 + q^2)\psi(\zeta), \quad (8)$$

where $\zeta = x/\Delta$ and the operator is $\hat{H} = -d^2/d\zeta^2 + 1 - 2\mathrm{sech}^2(\zeta)$. The eigenvalues $1 + q^2 = \omega/(\gamma_0\tilde{K})$ define the spin wave dispersion relation inside the DW, which is plotted in Fig. 1(c) (dark slate blue line) with wave vector $k = q/\Delta$. The above discussion is only valid for wavelengths smaller than the domain-wall size, which corresponds to wave vectors greater than $k_m \sim 1/(2\Delta)$. The propagating wave excitations can be expressed as $\psi(\zeta, t) = \rho_k e^{i\Omega}(\tanh(\zeta) - iq)$ where $\Omega = \zeta q - \omega t$ represents the sine or cosine type waves and ρ_k the wave vector dependent spin wave amplitude [29]. The reflectionless property for spin waves holds even in the presence of the easy plane anisotropy [30]. Interestingly, the dispersion relation inside the DW is symmetric in the reduced wave vector q even though the wall is twisted by the DMI. However, due to the

exponential decay of the DW profile when moving away from the DW center, the magnetization is uniform in the domains and the dispersion relations become asymmetric outside the DW [19,31],

$$\omega_{\pm} = \gamma_0(K + Ak^2 \pm Dk). \tag{9}$$

Figure 1(c) shows the asymmetric dispersion relations outside the DW. The dispersion relation [Eq. (9)] also suggests that the wave vector changes by D/A when the spin wave passes through the DW if the frequency of the spin wave remains the same. The spin wave becomes elliptical rather than circular if $K_\perp > 0$ and the corresponding dispersion relation outside the DW becomes $\omega_{\pm} = \gamma_0[\sqrt{(K + Ak^2)(K + K_\perp + Ak^2)} \pm Dk]$ [19].

To study the DW dynamics, micromagnetic simulations have been performed using a 1D mesh with length 2000 nm and cell size 1 nm. We make use of the parameters of FeGe [32]: the exchange constant $A = 8.78 \times 10^{-12}$ J/m, the DMI constant $|D| = 1.58 \times 10^{-3}$ J/m^2, the saturation magnetization $M_s = 3.84 \times 10^5$ A/m, and the damping coefficient $\alpha = 0.01$. We set the easy axis anisotropy $K = 1 \times 10^5$ J/m^3 and treat $K_\perp$ as an adjustable parameter since both anisotropies depend on the sample shape, strain, and surface effects [33]. The spin waves are excited locally in the region $-1000 \le x \le -998$ nm by a linearly polarized field $\mathbf{h}(t) = h_0 \sin(2\pi f t)\mathbf{e}_y$ with $h_0 = 1 \times 10^5$ A/m. The initial domain wall is located at $x_0 = 0$, and to prevent spin wave reflection the damping coefficient is increased linearly [10] from 0.01 to 0.5 in the region $800 \le x \le 1000$ nm.

The spin wave traveling in the $+x$ direction induces DW motion. Figure 2 shows the DW velocity as a function of frequency with different DMI constants for $K_\perp = 0$.

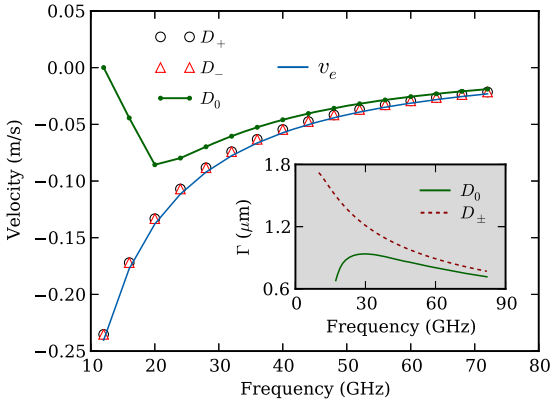

FIG. 2 (color online). Simulation results of the DW velocity as a function of spin wave frequency with different DMI constants for the case of $K_\perp = 0$. The DMI parameters are $D_0 = 0$ and $D_\pm = \pm 1.58 \times 10^{-3}$ J/m^2. The v_e curve is calculated by $v_e = -(\rho^2/2)V_g$ [11] where ρ at $x = 0$ is extracted from the simulation. Inset: Plot of spin wave amplitude decaying characteristic length Γ versus frequency.

The DW velocity is negative, which is explained by the conservation of angular momentum, and the DW velocity is $v_e = -(\rho^2/2)V_g$ [11], where $V_g = \partial\omega_k/\partial k$ is the spin wave group velocity and ρ is the spin-wave amplitude. For a circular spin wave, i.e., for $K_\perp = 0$, by using the dispersion relation inside the DW or Eq. (9) we have $V_g = 2\gamma_0 Ak = 2\sqrt{\gamma_0 A(\omega - \gamma_0\tilde{K})}$. In the absence of the DMI, the DW velocity is zero if the frequency is less than the cut-off frequency $f_{\rm cut} = \gamma_0 K \approx 14.5$ GHz, which is reduced to $\gamma_0\tilde{K} \approx 4.2$ GHz by the DMI. The magnitude of the DW velocity first increases, and then decreases as the frequency of the spin wave increases. The reason for this is that the spin wave amplitude decays exponentially as the spin wave propagates. To quantify this, we assume the magnetization has the form $\mathbf{m} = \pm\mathbf{e}_x + \boldsymbol{\rho_0} e^{i(kx-\omega t)} e^{-x/\Gamma}$ with $|\boldsymbol{\rho_0}| \ll 1$ [19,34], and obtain $\Gamma_\pm = 2/(\alpha\omega)[\gamma_0 Ak \pm D(\omega \mp D\gamma_0 k)/(K_\perp + 2K + 2Ak^2)]$, which is plotted in the inset of Fig. 2 with $K_\perp = 0$ and shows that the spin wave amplitude decaying is reduced by the existence of the DMI. The predicted DW velocity v_e is plotted in Fig. 2 as well, which fits the simulation results very well.

We now repeat the study for Fig. 2 above with $K_\perp > 0$ and where the spin waves are elliptical. Figure 3 shows the DW velocity as a function of spin wave frequency for $K_\perp = 2 \times 10^5$ J/m^3, and the corresponding DW displacements are shown in Fig. S1 (see Supplemental Material [26]). As in the $K_\perp = 0$ case, we find no spin wave reflection, and the DW velocity is negative if the DMI constant D is > 0. Similar to the $K_\perp = 0$ case, the DW velocity is zero when frequency $f < f_{\rm cut} \approx 16$ GHz, and the DW velocity first increases, and then decreases with the frequency. However, the magnitudes are significantly larger, and for the $D < 0$ case the DW velocity is positive.

To understand this novel DMI induced linear momentum transfer phenomenon, we recall the dispersion relation

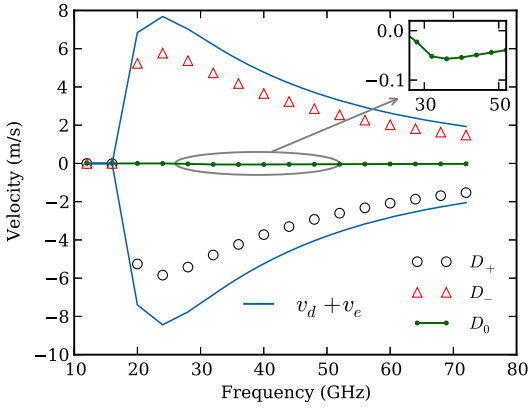

FIG. 3 (color online). The DW velocity as a function of the spin wave frequency with $K_\perp = 2 \times 10^5$ J/m^3. The DMI constants employed in the simulation are $D_0 = 0$ and $D_\pm = \pm 1.58 \times 10^{-3}$ J/m^2.

[Eq. (9)] outside the DW and assume the wave vector of a magnon before and after passing through the DW to be k_1 and k_2, respectively. When spin waves travel though the DW, they jump from branch ω_+ to ω_- in the dispersion relation, as depicted in Fig. 1(c) or Fig. S2(a) in Ref. [26]. By assuming the frequency keeps the same, the change in wave vector $\delta k = k_2 - k_1$ can be calculated. We show in Fig. S3(a) [26] that the frequency does not change significantly for our system. The change in wave vector δk leads to a momentum change $\delta p = \hbar \delta k$ for each magnon.

The excited magnon density is $n = \rho^2 M_s/(2\hbar\gamma)$ [12] and for elliptical spin waves we choose $\rho^2 = u_0 v_0$ where u_0, v_0 are fluctuation amplitudes in $\mathbf{e}_\theta$ and $\mathbf{e}_\phi$. The linear momentum of a DW is $P_{\mathrm{DW}} = M_s/\gamma \int \phi \sin\theta (\partial\theta/\partial x) dx = 2\Phi M_s/\gamma$ [35] and conservation of linear momentum [15] gives $dP_{\mathrm{DW}}/dt = -dP_{\mathrm{magnons}}/dt = -nV_g \delta p$, i.e., $\dot{\Phi} = -(1/4)\rho^2 V_g \delta k$. To describe the domain-wall motion, we introduce an effective field along the x direction by using the spherical form of the LLG equation,

$$H_x = \dot{\Phi}/\gamma = -\frac{1}{4}\rho^2 \delta k V_g/\gamma. \tag{10}$$

For circular spin waves $\delta k = D/A$, and thus the corresponding effective field is $H_x^0 = -(\rho^2/2)Dk\gamma_0/\gamma$. In the $\kappa > 0$ case (i.e., for $K_\perp > 0$), the spin wave is elliptical and δk is a function of the frequency (see Fig. S2 in the Supplemental Material [26]). The presence of a nonzero $K_\perp$ suppresses the wave vector change, especially for low frequency spin waves. The DW velocity v_d induced by this effective field H_x in the presence of damping can be obtained using the rigid DW model [36],

$$v_d = \frac{\gamma \Delta H_x}{\alpha} \Big/ \sqrt{1 + \frac{\kappa}{2}(1 - \sqrt{1-h^2})}, \tag{11}$$

where $h = H_x/(\alpha H_{K_\perp})$ and $H_{K_\perp} = 2K_\perp/(\mu_0 M_s)$. The total velocity is the sum of the established v_d and v_e, which correspond to the linear and angular momentum conservation, respectively.

To estimate the total velocity $v_e + v_d$, we have extracted the spin wave amplitude ρ at $x = 0$ (the initial position of the domain wall) from the simulation and the constant DW width Δ_0 is used. This total velocity is shown as lines in Fig. 3 and shows a good agreement with the simulation results shown as circle and triangle symbols. The maximum DW velocity is around $f = 24$ GHz, which originates from the combined dependencies of V_g, Γ and δk. Figure S2(b) shows that δk does not change significantly as the frequency increases. The DW can rotate freely if $K_\perp = 0$ and the DW velocity induced by the field H_x is $v_0 = \alpha\Delta\gamma_0 H_x/(1+\alpha^2)$. We can establish that $v_0 \sim 10^{-4}$ m/s, which could explain why the linear momentum exchange is not significant for the DW motion shown in Fig. 2.

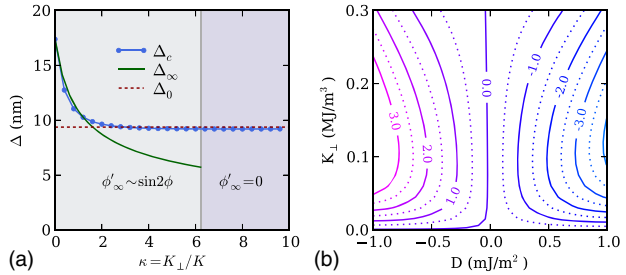

FIG. 4 (color online). (a) Plot of two types of domain walls, Δ_c is obtained by fitting the simulation data with $\cos\theta = -\tanh(x/\Delta_c)$. (b) The contour plot of the simulated DW velocity (in m/s) for different $K_\perp$ and DMI constants, where the frequency of the external ac field is fixed at $f = 30$ GHz.

The domain-wall width Δ is not a constant for the $K_\perp > 0$ case, and the corresponding DW profiles are described by Eq. (4). Using the asymptotic behavior of Eq. (4) (see Supplemental Material [26]) we can identify two types of domain walls when $K_\perp > 0$ and $D \neq 0$. The first type of DW is $\phi'_\infty = 0$ which corresponds to the small $|D|$ case with $\kappa > 0$, as shown in Fig. 4(a). The second type is $\phi'_\infty \sim \sin 2\phi$ where ϕ is a monotonic function. In this scenario, the DW width Δ_∞ for $x \to \infty$ is given by $1/\Delta_\infty^2 = (1 + \kappa/2 + \sqrt{1+\kappa})K/(2A) - 1/\xi^2$. From Fig. 4(a) we can find that Δ_∞ is a good approximation if $\kappa < 2$. The critical κ_c can be obtained by solving the equation $AK\kappa_c^2 = 2D^2(1 + \kappa_c/2 + \sqrt{1+\kappa_c})$, which gives $\kappa_c \approx 6.2$. The simulation results also show that for $\kappa \gg 1$ the DW width Δ_c is close to Δ_0.

So far the effective field is introduced by linear momentum conservation. In the following section we cross-check this using the LLG equation. The LLG equation [Eq. (2)] with zero damping is rewritten to describe the spin conservation law [37],

$$\frac{\partial \mathbf{m}}{\partial t} + \frac{\partial \mathbf{j}_e}{\partial x} = \boldsymbol{\tau}_a + \boldsymbol{\tau}_d, \tag{12}$$

where $\mathbf{j}_e = \gamma_0 A \mathbf{m} \times \partial_x \mathbf{m}$ is the exchange spin current associated with localized spin. The spin source or sink $\boldsymbol{\tau}_a = -\gamma_0 \mathbf{m} \times [K m_x \mathbf{e}_x - K_\perp m_z \mathbf{e}_z]$ and $\boldsymbol{\tau}_d = \gamma_0 D \mathbf{m} \times (\nabla \times \mathbf{m})$ come from the anisotropy and DMI, respectively. The average DW velocity can be computed through $v = (1/2)\int \langle \partial m_x/\partial t \rangle dx$ where $\langle f(t) \rangle$ represents the temporal average for a periodic function $f(t)$. To compute this average we keep the terms up to the square of the spin waves amplitude and ignore the higher-order ones. By integrating over space for the x component of the spin current $\mathbf{j}_e$, the velocity v_e can be recovered.

By using the DW profile [Eq. (5)] it is found that the overall contributions of the x component torques $\boldsymbol{\tau}_a$ and $\boldsymbol{\tau}_d$ are zero, i.e., $\int \langle \boldsymbol{\tau}_a^x \rangle dx = \int \langle \boldsymbol{\tau}_d^x \rangle dx = 0$. However, the contribution of the z component of the DMI torque is nonzero, i.e., $\int \langle \boldsymbol{\tau}_d^z \rangle dx = -\int (\rho^2/2)\gamma_0 D k m_y dx$, which represents an

additional torque rotating the DW plane. By introducing an effective field H_x^0 in the x direction such that the total torque on the DW equals the torque $\boldsymbol{\tau}_d^z$, we obtain $H_x^0 = \int \langle \boldsymbol{\tau}_d^z/\gamma \rangle dx / \int m_y dx = -(\rho^2/2) D k \gamma_0/\gamma$, which is in exact agreement with the analysis above.

Figure 4(b) shows a contour plot of the DW velocity as a function of $K_\perp$ and DMI constant D. The figure is approximately symmetric in the DMI constant, with a biased velocity originating from the angular momentum exchange between the spin wave and the DW. The DW velocity is always negative if $D > 0$. There exist some optimal areas in which the DW has the highest velocity, and this area depends on the frequency of the spin wave.

For a 2D magnetic sample, the magnetization at the edges is tilted due to the DMI, and the domain-wall velocity is slightly reduced compared to the 1D model used above (see Fig. S5 in the Supplemental Material [26]).

In conclusion, we have studied DMI induced linear momentum transfer DW motion. We find that the DMI exerts an extra torque which rotates the DW plane when the spin wave passes through the DW, and that the effective easy plane anisotropy suppresses the rotation and leads to a fast DW motion. The effect of the linear momentum is equivalent to an effective field and the direction of the field depends on the sign of the DMI constant and the DW profile. This linear momentum exchange between spin waves and the DW exists in addition to the angular momentum exchange when magnons pass through the DW, and is more efficient in moving the domain wall.

We acknowledge financial support from EPSRC's DTC Grant No. EP/G03690X/1. W. W thanks the China Scholarship Council for financial assistance.

*fangohr@soton.ac.uk

[1] D. A. Allwood, G. Xiong, C. C. Faulkner, D. Atkinson, D. Petit, and R. P. Cowburn, Science **309**, 1688 (2005).
[2] R. Hertel, W. Wulfhekel, and J. Kirschner, Phys. Rev. Lett. **93**, 257202 (2004).
[3] R. Wieser, U. Nowak, and K. D. Usadel, Phys. Rev. B **69**, 064401 (2004).
[4] S. S. P. Parkin, M. Hayashi, and L. Thomas, Science **320**, 190 (2008).
[5] B. Hu and X. R. Wang, Phys. Rev. Lett. **111**, 027205 (2013).
[6] N. L. Schryer and L. R. Walker, J. Appl. Phys. **45**, 5406 (1974).
[7] P. Yan and X. R. Wang, Phys. Rev. B **80**, 214426 (2009).
[8] S. Zhang and Z. Li, Phys. Rev. Lett. **93**, 127204 (2004).
[9] D. Hinzke and U. Nowak, Phys. Rev. Lett. **107**, 027205 (2011).
[10] D.-S. Han, S.-K. Kim, J.-Y. Lee, S. J. Hermsdoerfer, H. Schultheiss, B. Leven, and B. Hillebrands, Appl. Phys. Lett. **94**, 112502 (2009).
[11] P. Yan, X. S Wang, and X. R. Wang, Phys. Rev. Lett. **107**, 177207 (2011).
[12] X.-G. Wang, G.-H. Guo, Y.-Z. Nie, G.-F. Zhang, and Z.-X. Li, Phys. Rev. B **86**, 054445 (2012).
[13] X. S. Wang, P. Yan, Y. H. Shen, G. E. W. Bauer, and X. R. Wang, Phys. Rev. Lett. **109**, 167209 (2012).
[14] J.-S. Kim, M. Stärk, M. Kläui, J. Yoon, C.-Y. You, L. Lopez-Diaz, and E. Martinez, Phys. Rev. B **85**, 174428 (2012).
[15] P. Yan, A. Kamra, Y. Cao, and G. E. W. Bauer, Phys. Rev. B **88**, 144413 (2013).
[16] A. Janutka, IEEE Magn. Lett. **4**, 4000104 (2013).
[17] A. Fert, V. Cros, and J. Sampaio, Nat. Nanotechnol. **8**, 152 (2013).
[18] J. Zang, M. Mostovoy, J. H. Han, and N. Nagaosa, Phys. Rev. Lett. **107**, 136804 (2011).
[19] J.-H. Moon, S.-M. Seo, K.-J. Lee, K.-W. Kim, J. Ryu, H.-W. Lee, R. D. McMichael, and M. D. Stiles, Phys. Rev. B **88**, 184404 (2013).
[20] S. Rohart and A. Thiaville, Phys. Rev. B **88**, 184422 (2013).
[21] A. Thiaville, S. Rohart, E. Jué, V. Cros, and A. Fert, Europhys. Lett. **100**, 57002 (2012).
[22] O. A. Tretiakov and A. Abanov, Phys. Rev. Lett. **105**, 157201 (2010).
[23] S. Mühlbauer, B. Binz, F. Jonietz, C. Pfleiderer, A. Rosch, A. Neubauer, R. Georgii, and P. Böni, Science **323**, 915 (2009).
[24] S. X. Huang and C. L. Chien, Phys. Rev. Lett. **108**, 267201 (2012).
[25] N. A. Porter, J. C. Gartside, and C. H. Marrows, Phys. Rev. B **90**, 024403 (2014).
[26] See Supplemental Material at http://link.aps.org/supplemental/10.1103/PhysRevLett.114.087203 for details of the boundary conditions, the estimation of the domain wall width and the simulation results for a 2d sample.
[27] H.-B. Braun, Phys. Rev. B **50**, 16485 (1994).
[28] J. Lekner, Am. J. Phys. **75**, 1151 (2007).
[29] E. G. Tveten, A. Qaiumzadeh, and A. Brataas, Phys. Rev. Lett. **112**, 147204 (2014).
[30] P. Yan and G. E. W. Bauer, Phys. Rev. Lett. **109**, 087202 (2012).
[31] K. Zakeri, Y. Zhang, J. Prokop, T.-H. Chuang, N. Sakr, W. X. Tang, and J. Kirschner, Phys. Rev. Lett. **104**, 137203 (2010).
[32] M. Beg, D. Chernyshenko, M.-A. Bisotti, W. Wang, M. Albert, R. L. Stamps, and H. Fangohr, arXiv:1312.7665.
[33] E. A. Karhu, U. K. Rößler, A. N. Bogdanov, S. Kahwaji, B. J. Kirby, H. Fritzsche, M. D. Robertson, C. F. Majkrzak, and T. L. Monchesky, Phys. Rev. B **85**, 094429 (2012).
[34] S.-M. Seo, K.-J. Lee, H. Yang, and T. Ono, Phys. Rev. Lett. **102**, 147202 (2009).
[35] A. Kosevich, B. Ivanov, and A. Kovalev, Phys. Rep. **194**, 117 (1990).
[36] B. Hillebrands and A. Thiaville, *Spin Dynamics in Confined Magnetic Structures III* (Springer, New York, 2006).
[37] G. Tatara, H. Kohno, and J. Shibata, Phys. Rep. **468**, 213 (2008).